Title	Harmonic stability of VSC connected Low Frequency AC offshore transmission with long HVAC cables
Authors(s)	Ruddy, Jonathan, Chen, Junru, Meere, Ronan, O'Loughlin, Cathal, O'Donnell, Terence
Publication date	2018-09
Publication information	Ruddy, Jonathan, Junru Chen, Ronan Meere, Cathal O'Loughlin, and Terence O'Donnell. "Harmonic Stability of VSC Connected Low Frequency AC Offshore Transmission with Long HVAC Cables" 162 (September, 2018).
Publisher	Elsevier
Item record/more information	http://hdl.handle.net/10197/10451
Publisher's statement	This is the author's version of a work that was accepted for publication in Electric Power Systems Research. Changes resulting from the publishing process, such as peer review, editing, corrections, structural formatting, and other quality control mechanisms may not be reflected in this document. Changes may have been made to this work since it was submitted for publication. A definitive version was subsequently published in Electric Power Systems Research (162, (2018)) https://doi.org/10.1016/j.epsr.2018.05.017
Publisher's version (DOI)	10.1016/j.epsr.2018.05.017

Harmonic Stability of VSC Connected Low Frequency AC Offshore Transmission with Long HVAC Cables

J. Ruddy[a,*], J. Chen[a], R. Meere[b], C. O'Loughlin[a], T. O'Donnell[a]

[a]*Electrical Engineering Department, University College Dublin, Ireland*
[b]*ESB Networks, Dublin, Ireland*

Abstract

Low Frequency AC (LFAC) transmission has been proposed as an alternative to HVDC transmission for the integration of offshore wind. The LFAC offshore grid as a fully power electronic grid with a long HVAC cable provides significant challenges to harmonic stability. This paper presents an impedance based stability analysis to determine the stability of the power electronic offshore system across the harmonic frequency range. The stability analysis is introduced and applied to the LFAC system. The impact of different current and voltage control bandwidths and component sizes on the dynamic impedance of the converters is then examined and their impact on harmonic stability of the LFAC grid is determined. It is found that detailed knowledge of the control parameters and the ability to tune the bandwidths can mitigate significant harmonic instability with the presence of a long HVAC cable. Three phase simulations are then used to validated the impedance based stability technique.

Keywords: Low Frequency AC, Impedance measurement, Harmonic stability

1. Introduction

In recent years the development of offshore wind has increased dramatically. Consequently there has been a significant drive in research and industry to improve the competitiveness of offshore wind compared to other energy sources. Low Frequency AC (LFAC) transmission, typically at a frequency of 16.7 Hz has been proposed as an alternative to conventional 50 Hz AC or VSC-HVDC transmission [1, 2, 3]. LFAC is an interesting alternative transmission option for offshore wind, primarily due to the extension of AC power transmission distance at lower frequency. Offshore cables operated at low frequency (usually

16.7 Hz) extend the maximum power transmission distance of the cable from 60-80 km at 50 Hz to 180-200 km. The key advantage of LFAC compared to HVDC is the removal of the offshore power electronic converter station [1, 4]. The elimination of the offshore converter station is based on the assumption that the wind turbines have the ability to produce AC at a lower frequency [1], which is possible with full converter Type IV wind turbines. The LFAC transmission cable transmits power at low frequency to the shore where a frequency changing converter converts from low frequency to the grid frequency. This technology reduces the complexity offshore and therefore may reduce the capital investment costs and increase reliability, with the impact of decreasing the overall cost of offshore wind. LFAC has been used in the rail systems in parts of Europe for many years, trains operate at a frequency of 16.7 Hz and as such LFAC has an already established industry base, producing equipment at low frequency, albeit, primarily single phase and lower voltage. Potential drawbacks to LFAC transmission include the size of low frequency transformers and inductive elements at low frequency. A review of the research has shown that LFAC transmission is an economically competitive transmission option for offshore wind farms between 100 km and 200 km from shore [5]. The LFAC grid offshore is a fully power electronic defined grid where the onshore BtB converter in grid forming control mode establishes and maintains the offshore grid voltage. The offshore wind turbines synchronise to this grid via a Phase Locked Loop (PLL).

Power electronic grids provide advantages over traditional grids including full controllablity and improved efficiency. However, they also introduce new challenges. High frequency switching introduces harmonics which may interact with higher frequency resonances [6], also power converter control interactions may exist between converter controls and between control and passive components. In planning for large power electronic grids it is important to determine the stability of a system across a range of frequencies [7]. The first real experience with inverter dominated offshore grids has been BorWin1, a HVDC connected offshore wind farm in the North Sea [8]. Stability problems due to interaction of converters and grid resonances were observed and caused significant outages [8, 9]. These problems are of particular interest to an LFAC system due to the presence of very long HVAC cables.

A number of analysis methods exist to determine the stability of a system including passive harmonic impedance scans, eigenvalue analysis (requires a lot of detail about proprietary controllers and system variables) and full 3 phase time domain analysis. In generic power systems state space models are developed to determine stability, where the dynamics are primarily dictated by rotating machines. However, with power electronics the fast dynamics of controllers and non linearity's require more detailed state space modelling of loads and the network to understand their dynamic response to the much smaller system time constants [6]. An approach to overcome this limitation is the Component Connection Method (CCM) where the power system components and network dynamics are separately modelled by a set of vector-matrix equations [10]. CCM is a particular form of state space analysis which reduces state equations to lessen the computation burden. The separation allows the interactions and critical parameters to be more easily determined [6]. A state space approach to stability in power electronic grids would require full detail of the dynamics of the mechanical and electrical subsystems involved in the wind farm. In a real system this

may not be applicable due to the complexity of wind turbine control and the unavailability of data about these subsystems [9].

Impedance based analysis provides a practical tool for the assessment of stability in power electronics based power systems. The impedance measurement approach separates the system into source and load subsystems and examines the interaction between the two subsystems [11]. The impedances in general are composed of contributions from the converter controllers and the actual physical impedances. The impedance can be measured in the abc (positive and negative sequence) frame [12, 9, 6, 13], or dq domain [14, 15, 16] which may have advantages from the perspective of control analysis. Reference [14] proves mathematically the relationship between the two domains and shows that both can be viewed equally as a method for stability analysis. An assumption present in the majority of sequence impedance analysis to date is that the positive and negative sequence impedances of the inverters are decoupled from each other. This is true if the inner current and voltage control loops of the inverters have symmetric structures and equal parameters and if there is no PLL or the PLL has a low enough bandwidth that it's effect is negligible. Under these conditions impedance measurement for stability has been used to determine the harmonic stability between HVDC converters and offshore wind farms [17, 18] and the stability of systems with multiple power electronic inverters [6, 14, 19].

In contrast to the state space approach which examines the eigen-properties of the state matrix, the impedance measurement predicts system stability based on the ratio of the output and load impedance. A comparison of the state space approach and the impedance based approach can be found in [20], concluding that both methods are applicable for the determination of system stability. The advantages of the impedance based approach are that the impedance data is measured data from the real system and can potentially be measured on-line [21]. Impedance measurement is a more straightforward approach for power system planners than eigenvalue analysis or CCM as the unavailability of proprietary information from vendors is not a critical issue, provided accurate impedance data is supplied, or there is the ability to take measurements.

In addition to its practical advantages the impedance stability approach has proved to be an intuitive approach to determining stability. The first applications of the method involved the investigation of stability in cascaded dc-dc converter systems [22, 23]. In recent years there has been considerable interest for application in power systems as power electronics connected generation and transmission becomes more prevalent. For example, it has been used investigate the stability of paralleled inverters in systems with high penetrations of distributed generation [24] and as the basis for performing real time stability analysis in distribution systems [25]. The use of impedance stability analysis has also been employed to study various aspects of the stability of HVDC systems including the dc side stability [26, 27, 28], and the impacts of changing power flow directions [29]. Reference [30] provides a comprehensive overview of the impedance stability method and its applications. Considering these previous applications of the impedance stability method, it can be concluded that it provides a strong basis for investigation of the stability of the LFAC transmission system, which to the authors knowledge has not been done to date.

The key contribution of this paper is an investigation of the harmonic stability of an LFAC

offshore transmission system making use of the impedance based stability analysis approach. As noted above, the harmonic stability is of particular importance given that LFAC system is a converter based AC transmission system where the converters are interconnected using long HVAC cables. While some previous publications have made reference to potential harmonic issues, to the best of the authors knowledge this is the first time a thorough stability analysis has been performed for an LFAC transmission system. The approach accurately predicts the harmonic stability of the LFAC grid in the presence of long HVAC cables by examining interactions between the onshore BtB converter and the LFAC cable resonances. The factors affecting the stability of the power electronic grid are analysed including the parameters of the current and voltage controllers of the onshore BtB converter and the length of the LFAC cable. In addition the ability of the impedance method to predict harmonic instability is validated by application to a scaled hardware version of the LFAC transmission system.

2. Control of LFAC transmission system

Figure 1 displays the layout of an LFAC transmission system. Offshore, type IV wind turbines are used and the power is collected by a 16.7 Hz collector system. At the AC platform an LFAC transformer connects the offshore wind farm to the LFAC cable. In this analysis the wind turbine converters are lumped into one large converter representing the offshore wind farm. Onshore, the frequency is converted from 16.7 Hz to 50 Hz via a BtB converter onshore. The BtB converter is comprised of two Voltage Source Converters (VSC). The VSC on the low frequency side is required to establish and maintain the offshore low frequency voltage. The LFAC system is unique in the fact that it comprises a fully power electronic grid offshore, fed by power electronic inverters and includes a long AC cable with low frequency resonant points providing potential harmonic stability issues.
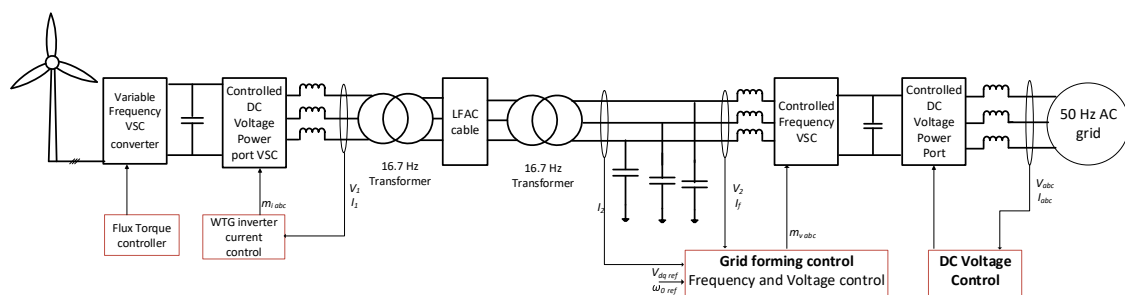

Figure 1: LFAC transmission system.

Figure 2 outlines the control schemes used in this analysis for the current controlled inverter and the voltage controlled inverter.

2.1. Voltage Control Scheme

The voltage control scheme shown in Figure 3a inputs a reference dq voltage, which is compared to the measured dq voltage at the capacitor of the LC filter. An output reference current is added to a feed forward measurement to provide the reference i_{dq} for the dq current control scheme.
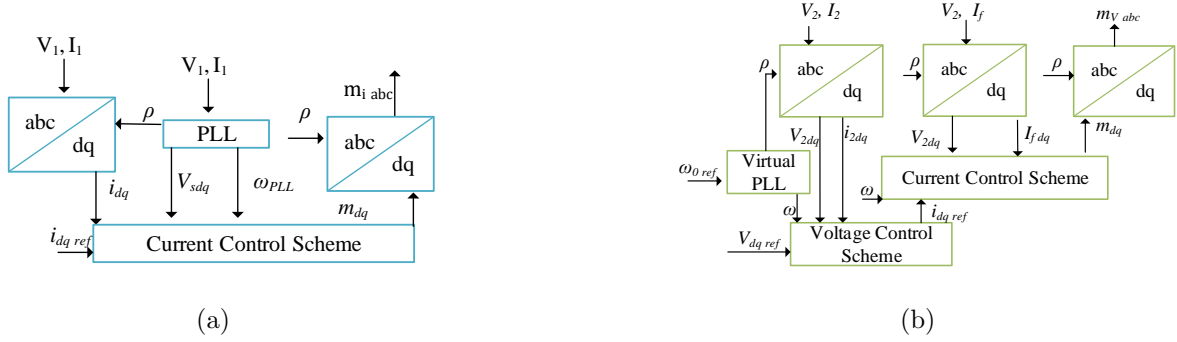
4

Figure 2: Control schemes of (a) current controlled inverter and (b) voltage source inverter.
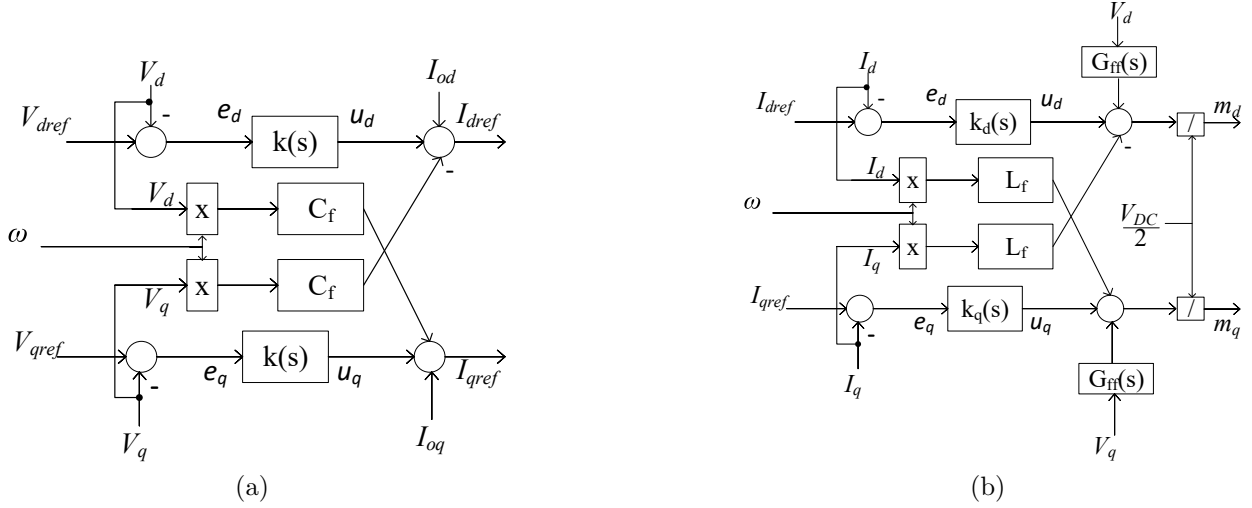

Figure 3: Control schematics of (a) voltage control Scheme block and (b) dq current control scheme block.

The compensator $k(s)$ is a PI controller:

$$k(s) = K_{pv} + \frac{K_{iv}}{s} = k\frac{s+z}{s} \tag{1}$$

In this paper it is assumed z is a zero which is dependent on the current controller time constant and the phase margin chosen for the voltage controller [31]. The compensator gain k is obtained from the solution of Equation 2 where ω_c is the required bandwidth of the voltage controller, C_f, C_c and n are the filter capacitance, cable capacitance and transformer turns ratio.

$$k = (C_f + n(C_c))\omega_c \tag{2}$$

2.2. Current Control Scheme

Figure 3b outlines the structure of the inner dq current control block of Figure 2a. The objective is to regulate the dq currents, i_d and i_q to their reference values. The value of L_f in the control is the interface reactor inductance. Typically $k_d(s)$ and $k_q(s)$ are PI controllers, which are designed according to Equations 3 - 5

$$k_d(s) = k_q(s) = \frac{K_p s + K_i}{s} \tag{3}$$

$$K_p = \frac{L_f}{t_i} \tag{4}$$

$$K_i = \frac{R + R_{on}}{t_i} \tag{5}$$

K_p and K_i are the proportional and integral constants, respectively. These constants are chosen according to the desired system time constant, t_i, phase reactor resistances and turn on resistance for IGBTs, $(R + R_{on})$, and phase reactor inductance, L_f.

3. Stability Analysis by Impedance Measurement

The basis of the impedance measurement based stability criteria is to split the system into a source and load subsystem. The source subsystem of a voltage controlled inverter consists of a Thevenin equivalent circuit with an ideal voltage source in series with an output impedance $(Z_s(s))$. The load subsystem is modeled by its load impedance $(Z_L(s))$. For the current controlled inverter based system the source subsystem consists of a Norton equivalent circuit with an ideal current source in parallel with an output admittance $(Y_s(s))$. The load subsystem is modeled by its input admittance $(Y_L(s))$. Figures 4a and 4b depict the equivalent small signal circuit of voltage controlled converter and current controlled inverter for impedance based analysis [11]. In Figure 4 $G_{cl}(s)$ is the closed loop reference to output transfer function which controls the dynamics of the inverters.

Equations 7 and 6 show the closed loop transfer functions of the inverter small signal systems in Figure 4. On the assumption that $G_{clv}(s)$ and $G_{cli}(s)$ are independently stable the stability of the output of both the voltage controlled inverter and the current controlled converter is dependent on the minor loop feedback of $\dfrac{Z_s(s)}{Z_L(s)}$ and $\dfrac{Y_s(s)}{Y_L(s)}$. Based on these minor feedback gains the stability of the system can be determined.

$$\frac{V_2(s)}{V_2^*(s)} = G_{clv}(s)\frac{1}{1 + \frac{Z_s(s)}{Z_L(s)}} \tag{6}$$

$$\frac{I_1(s)}{I_1^*(s)} = G_{cli}(s)\frac{1}{1 + \frac{Y_s(s)}{Y_L(s)}} \tag{7}$$

The source and load impedances and admittances can be found by injecting perturbations at the connection point between the subsystems. The resulting impedances across
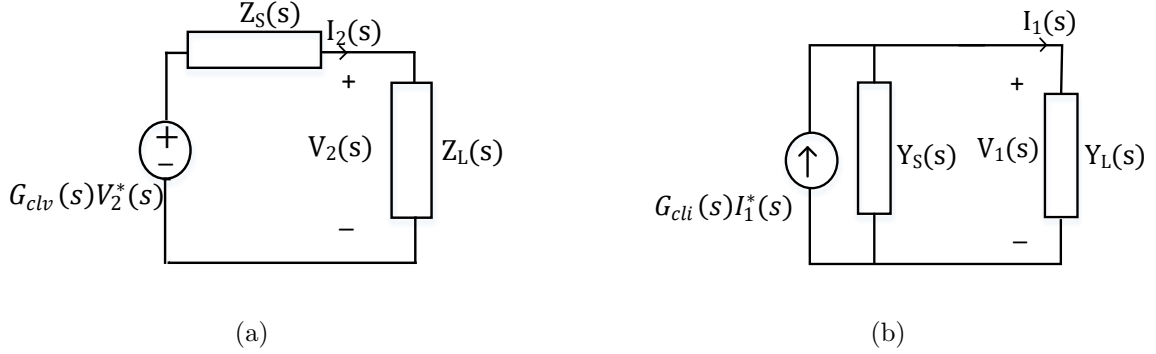
6

Figure 4: Small signal representation of (a) voltage source inverter with a load and (b) current source inverter with a load.

a frequency range can be examined to identify potentially unstable frequencies for a wide range of operating conditions.

3.1. LFAC Impedance Scan Technique

Figure 5 represents an extension of Figure 4a where the load impedance is replaced by the LFAC cable and the LFAC transformers $(Z_{cable}(s))$ and the impedance of the current controlled inverter $(Z_c(s))$. Figure 6 display the small signal representation of the setup to determine the stability of the current controlled inverter, showing the components of the load admittance. The stability of each inverter is assessed separately using the appropriate circuit setup.
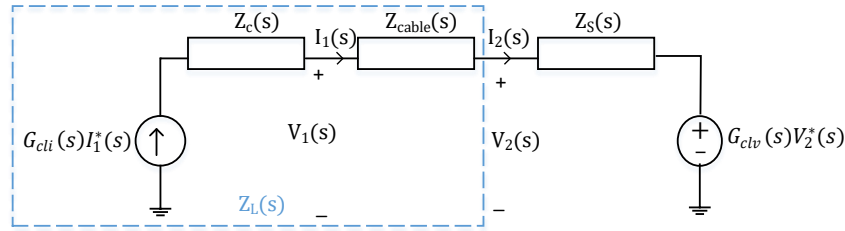

Figure 5: Small signal representation of $Z_s(s)$ and $Z_L(s)$ to find the stability of the LFAC voltage controlled inverter.

In both cases the load subsystem $(Z_L(s)$ and $Y_L(s))$ includes the LFAC transmission cable and the LFAC transformers. Similar to Figure 4 the stability of the LFAC transmission system depends on the stability of the minor loop feedback of $\dfrac{Z_s(s)}{Z_L(s)}$ and $\dfrac{Y_s(s)}{Y_L(s)}$ for each inverter. The LFAC system is split into two subsystems at the point of connection of the onshore converter to the offshore grid. Figure 7 shows the single line diagrams of the circuit setup to obtain the impedance measurement $Z_s(s)$ and $Z_L(s)$. Figure 8 displays the circuit
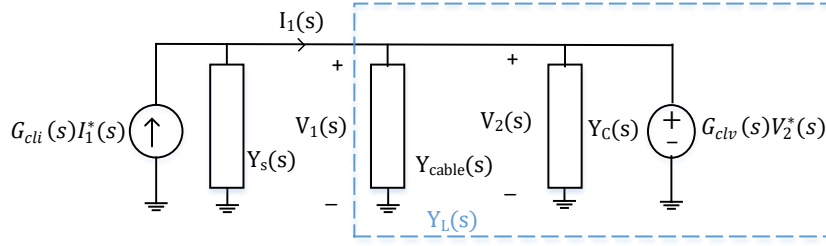
7

Figure 6: Small signal representation of $Y_s(s)$ and $Y_l(s)$ inverter with a cable and load.

setup used to determine $Y_s(s)$ and $Y_L(s)$. For both voltage controlled converter cases (Figures 7a and 8b) the subsystem is connected to a stiff current source, at 1 pu, corresponding to full loading, at the fundamental frequency of 16.7 Hz (ω_0). A current perturbation is added at a disturbance frequency of ω_d and an amplitude of 0.01 pu to maintain the small signal integrity of the model. The voltages and currents at the input perturbation can be measured and a Fast Fourier Transform (FFT) performed on them to identify the voltage and current components at ω_d and the impedance or admittance can be calculated from the measured voltages and currents.
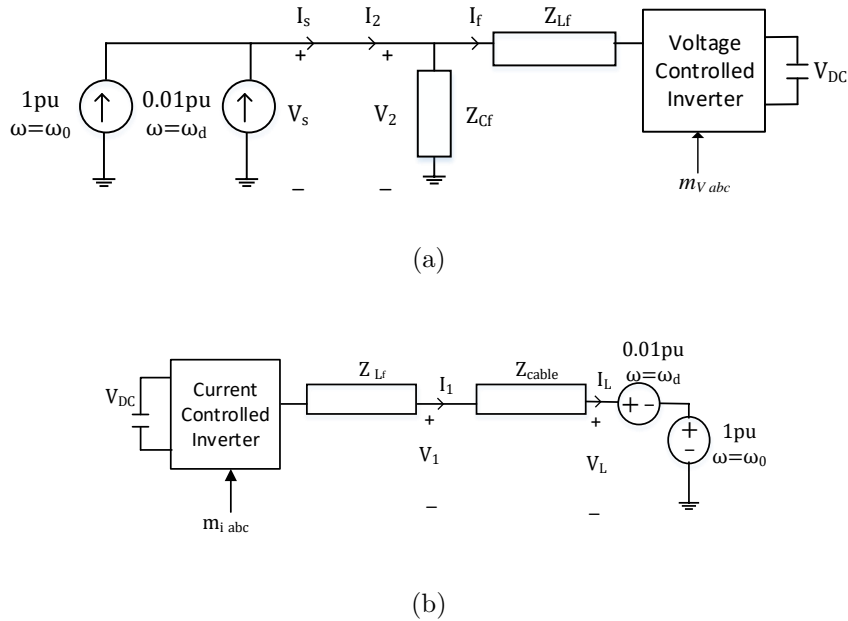

(a)

(b)

Figure 7: Single line diagram of impedance measurement circuit setup to find (a) Z_s and (b) Z_L.

Similarly for the current controlled inverter side (Figures 7b and 8a) the subsystem is connected to a stiff voltage source and a voltage perturbation is added at ω_d. Figure 9 displays a flowchart of the methodology for performing the impedance measurement to

8

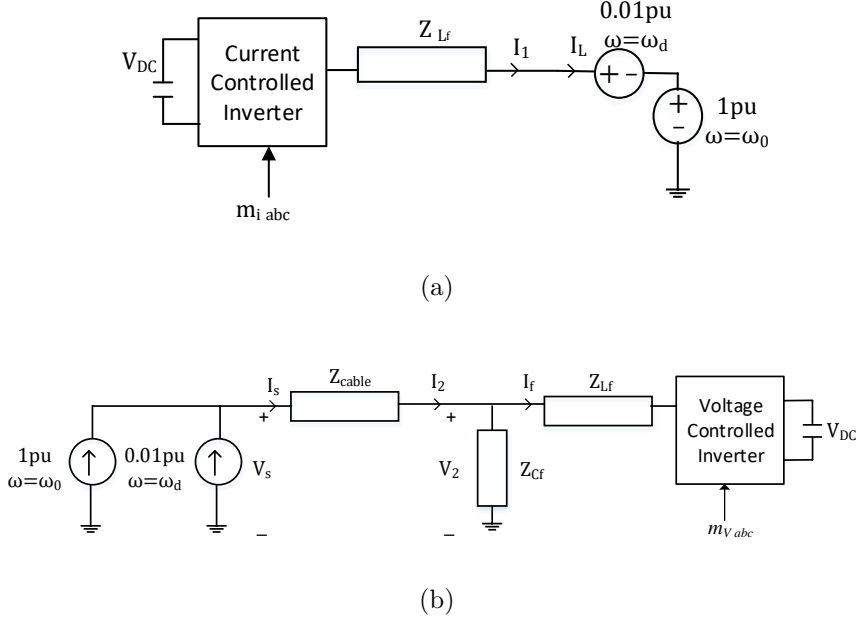calculate the admittance or impedance as required.

(a)

(b)

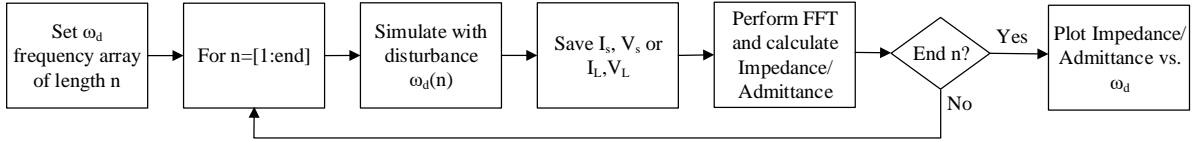Figure 8: Single line diagram of impedance measurement circuit to find (a) Y_L and (b) Y_s.

Figure 9: Flowchart methodology for determining impedance and admittance.

3.2. Voltage Controlled Inverter Impedance

In order to give some insight into the origin of the impedance curves and as a form of validation, the obtained impedance scans are first compared to the physical impedances of the cable, transformers and filters connected to an open circuit, without the influence of converter control. The parameters used in this analysis are outlined in Table 1. In Figure 10 the measured impedance Z_L is compared to the impedance of the cable, transformers wind farm inductance and VSC, without the influence of the controllers. It can be clearly seen from Figure 10 that the impedance scan matches the physical impedance outside of the bandwidth of the current control loop. Within the current control bandwidth the impedance rises as frequency approaches zero, which is expected for a current controlled inverter. For an ideal current controller the impedance at the fundamental frequency is equal to the unloaded cable impedance, as at this frequency the controller allows no disturbance current.

9

Parameter	Value
Voltage Controller Bandwidth (ω_c)	334.2 rads^{-1}
Voltage Controller (K_p,K_i)	0.0113, 1.2628
Current Controller Bandwidth ($\frac{1}{t_i}$)	1000 rads^{-1}
Current Controller (K_p,K_i)	85.77, 181.82
Filter Inductance (L_f)	85.8 mH
Filter Capacitance (C_f)	4.03 μF
Cable Inductance	222.8 μH/km
Cable Capacitance	198 nF/km
Transformer turns ratio	2.2:1
V_{DC}	400 kV
$V_{sd}ref$, $V_{sq}ref$	100 kV, 0 V
I_d reference	1000 A

Table 1: LFAC transmission system parameters for impedance measurements.

The first LC resonance associated with L_f and the cable capacitance falls within the current control bandwidth and is therefore not present in the impedance measurement as it has been controlled out.
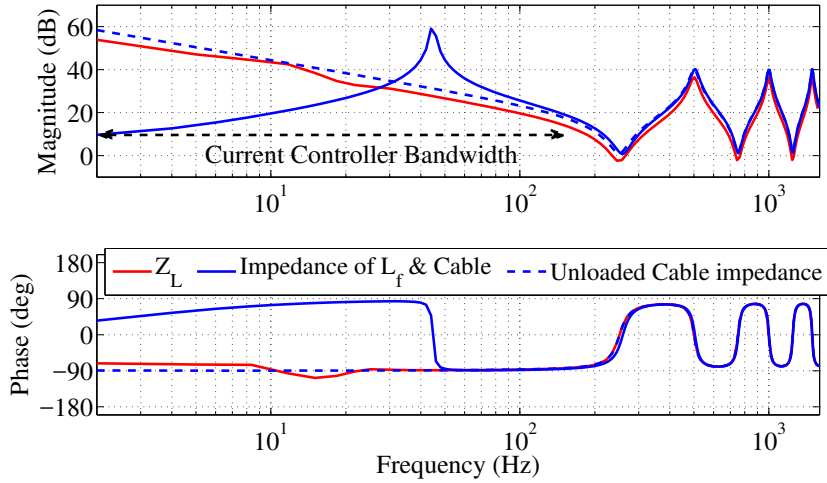

Figure 10: Comparison of directly measured impedance of 150 km cable and wind farm inductance with impedance Z_L.

Similarly Figure 11 displays the measured impedance of Z_s compared to the impedance of the LC filter. At frequencies above the current controller bandwidth the impedance is dominated by the capacitor in the LC filter. Again within the current control bandwidth the current controller dominates the dynamic impedance. The influence of the voltage controller can be seen where Z_s tends to go to zero at the fundamental, 16.7 Hz. This is due to the

integrator in the voltage controller and the fact that at the fundamental frequency in the *abc* frame, the *dq* component is at 0 Hz. Therefore 1/s becomes infinite, implying infinite gain which results in zero impedance. Below the fundamental frequency the frequency in the *dq* frame is negative which is treated the same as the equivalent positive one by the voltage controller and the impedance from zero to the fundamental mirrors the impedance from the fundamental to twice the fundamental. For example, a disturbance at $\omega_d = 5$ Hz, corresponds to -11.7 Hz in the *dq* frame. The voltage controller responds in the same way as for 11.7 Hz. Converting this back to the *abc* frame gives the same response as $\omega_d = 28.4$ Hz.
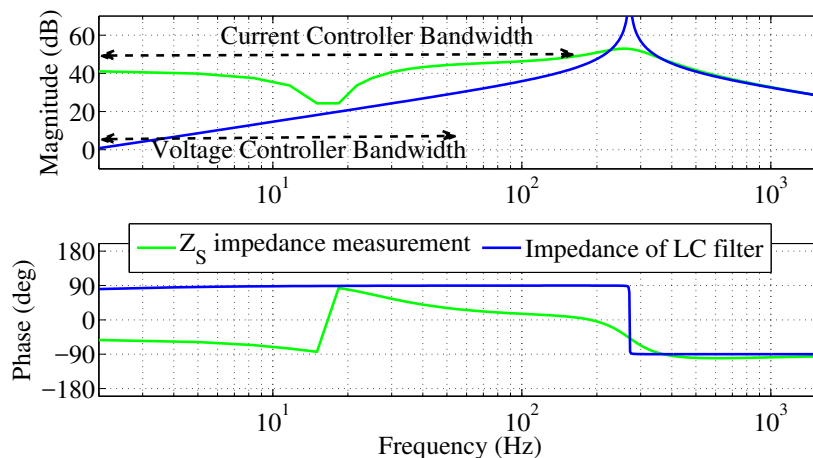

Figure 11: Comparison of directly measured impedance of LC filter with impedance Z_s.

3.3. Current Controlled Inverter Impedance

Figure 12 show the source and load admittance of the current controlled inverter system which has the PLL included in the source admittance. The factors which effect the source admittance in the lower frequency range are the PLL, the current controller and the inductive filter.

The effect of the PLL is to cause a decrease in the source impedance resulting in an increased admittance [32]. The factors which impact the load admittance are the voltage and current controllers and the LFAC cable. Decreasing the voltage control bandwidth decreases the load admittance. It can be clearly seen that the combined phase in the high frequency range cannot be below -180°, indicating the minor loop response will be stable and therefore the current controlled inverter has no harmonic stability issues resulting from the LFAC cable.

4. Harmonic Stability of LFAC transmission

Harmonic instability in power electronic grids can be caused by a combination of factors. These include fast inner current or voltage controllers and high frequency switching harmonics interacting with passive elements in the grid such as capacitors, filters or underground
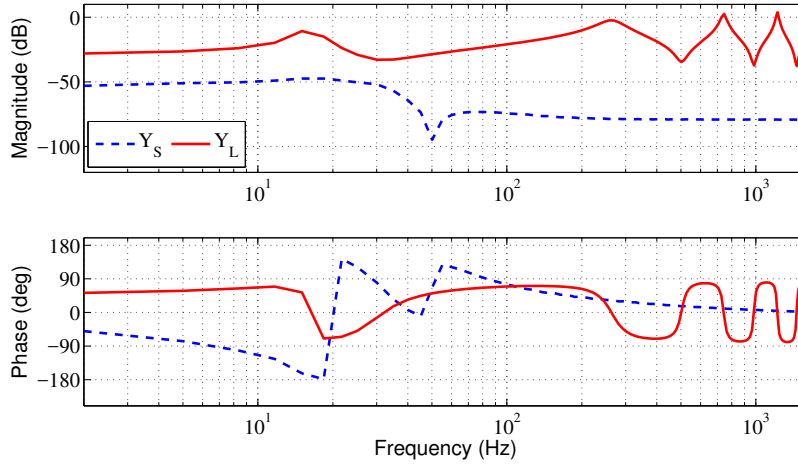
11

Figure 12: Source and load admittance of current controlled inverter.

cables [13]. The aspects of interest in an LFAC grid are the current and voltage controllers of the onshore voltage controlled converter, the LC output filter and the LFAC cable. In this harmonic analysis the stability of the voltage controlled converter is analysed by examining the minor loop response of Z_L and Z_S and their variation with capacitance in the offshore grid, the length of the LFAC cable and control parameters. The load impedance consists of the LFAC cable and the wind farm current controlled inverter.

4.1. Impact of Filter Capacitance

Initially the current controller bandwidth for the voltage controlled inverter is set to 2000 rads^{-1}. Figure 13 displays the load and source impedances for the voltage controlled inverter with a 100 km cable. To illustrate the effect of filter parameters, in Figure 13 the filter capacitance C_f is changed from 4 μF to 11 μF. This has the impact of decreasing Z_s above the LC corner frequency and therefore causing Z_s and Z_L to cross at more points, increasing the chance of the system becoming unstable when connected to the load subsystem which includes the LFAC cable.

Figure 14 shows the minor loop response of both scenarios. The minor loop magnitude is the ratio of $\dfrac{Z_S}{Z_L}$ and the phase is the difference of the angles at the given frequency. For the minor loop response and the inverter to be stable, when the minor loop magnitude is equal to 0 dB, i.e. $|Z_S| = |Z_L|$, the phase must be greater than -180°.

It can be seen from the minor loop plot that the combined impedance crosses 0 dB at the frequencies and phases outlined in Table 2 and that the 11 μF capacitor causes an instability at 1372 Hz. Decreasing the capacitance to 4 μF increases the impedance Z_s, thereby increasing the minor loop response and removing the instability.

4.2. Impact of Voltage Controller Bandwidth

An advantage of the impedance measurement approach is to measure the dynamic impedance of the converter including the impact of the control systems and their parame-
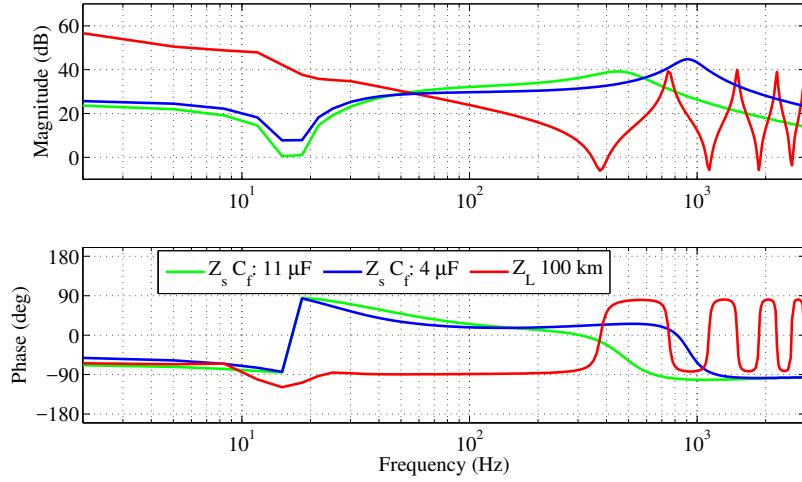
12

Figure 13: Impedance scans of voltage controlled side with changing filter capacitance compared to wind farm impedance with 100 km cable with current controller bandwidth 2000 rads $^{-1}$.
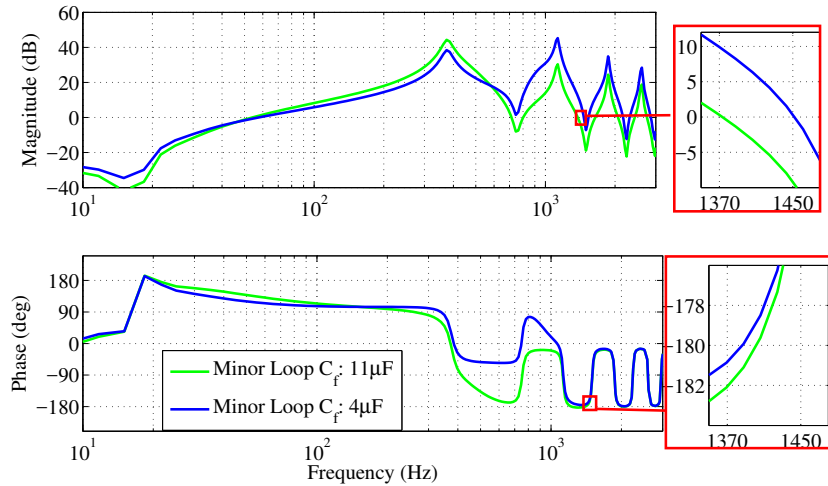

Figure 14: Minor loop responses varying filter capacitance with 100 km cable.

ters. Figure 15 shows the impact of changing the voltage control bandwidth on the source impedance. The control bandwidth is changed from 334 rad s^{-1} to 669 rad s^{-1}. It can be seen that in the lower frequency range the impedance is slightly reduced with a higher voltage control bandwidth. Outside of the current control bandwidth the impedance returns to the physical impedance of the LC filter.

4.3. Impact of Current Control Bandwidth

Figure 16 displays the impedance of the system again with an 11 μF capacitor. The impact of changing the current controller bandwidth is shown for two bandwidths, low (1000 rads^{-1}) to high (2000 rads^{-1}) for the voltage controlled inverter. The high control
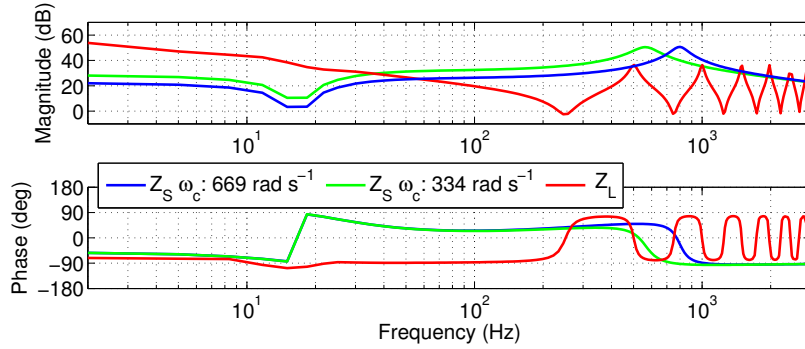
13

Figure 15: Z_L and Z_s for LFAC voltage controlled inverter.

bandwidth scenario here has the same parameters as the unstable scenario in Figure 13. It can be clearly seen in Figure 17 that the minor loop with high current controller bandwidth is unstable at a frequency of 1372 Hz and is stable for all frequencies with a low current control bandwidth. This shows the impact control parameters can have on harmonic stability. The minor loop response does cross 0 dB at other frequencies, however the phase in those cases is not below -180°. The frequencies at which the minor loop responses are equal to 0 dB and the corresponding phase angles are outlined in Table 2.
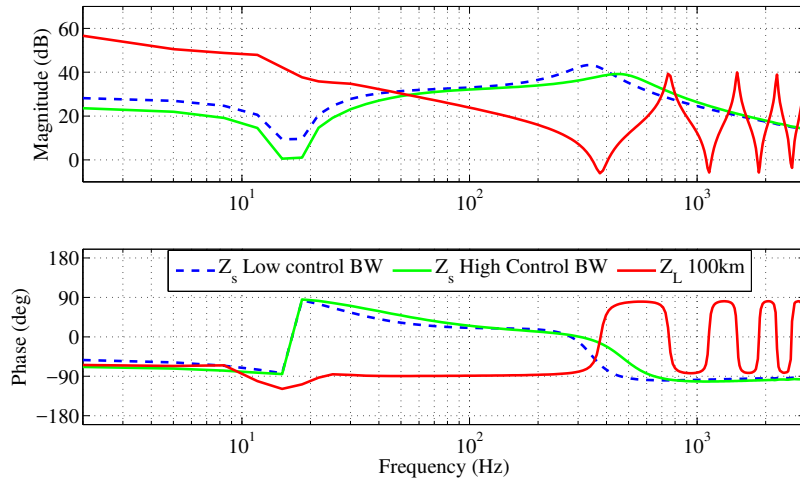

Figure 16: Impedance scans of voltage controlled with 11 μF C_f varying current controller bandwidth compared to wind farm impedance with 100 km cable.
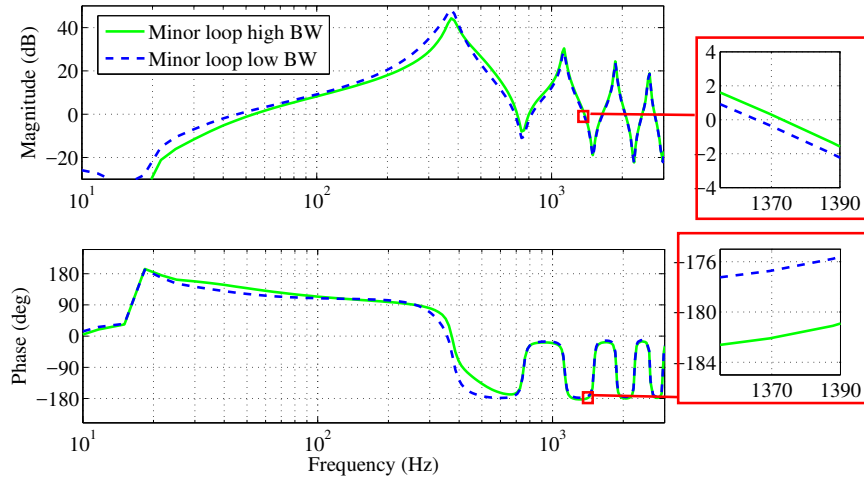
14

Figure 17: Minor loop responses with varied current controller bandwidth with 100 km cable, unstable for high current controller bandwidth and stable for low current controller bandwidth.

Table 2 summarises the responses shown in Figures 16 - 17, outlining the parameters changed and the responses observed at the stability points.

Figure	Z_s Current Control BandWidth, (K_p, K_i)	C_f	Z_L Cable Length	$\|\frac{Z_s}{Z_L}\| = 0$ dB Frequency (Hz)	Angle (degrees)
17	1000 rad s^{-1} (85.78, 181.8)	11 μF	100 km	689 830 1351	-174 -20 -177
14, 17	2000 rad s^{-1} (171.54, 363.6)	11 μF	100 km	700 818 1370	-172 -28 -182
14	2000 rad s^{-1} (171.54, 363.6)	4 μF	100 km	1450 1525	-168 -45

Table 2: Details of parameters used and the frequencies where minor loop responses are 0 dB below 1500 Hz.

4.4. Impact of Cable Length

It has been seen in Figures 13 and 16 that increasing current control bandwidth and filter capacitor size in isolation can have an adverse effect on stability.
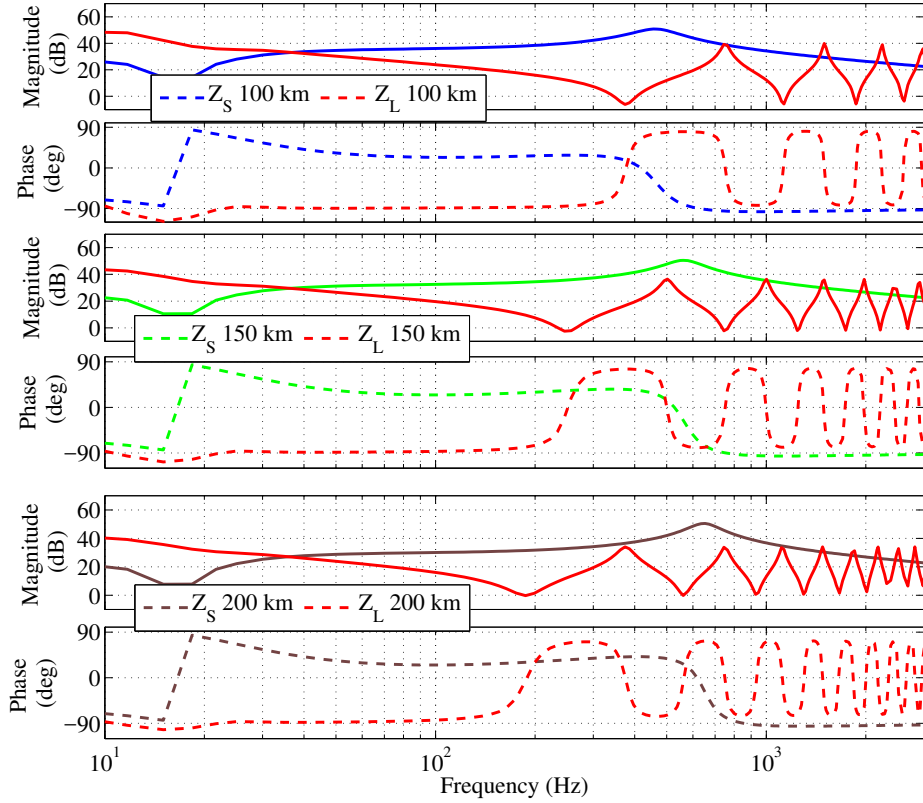
Figure 18: Source and load impedance for 3 cable lengths.

Figure 18 shows the source and load impedance for three different cable lengths with a current control bandwidth of 1000 rads^{-1}. Interestingly increasing the cable length appears to have a positive impact on harmonic stability in the LFAC case. For longer cables the resonant frequencies decrease to below or close to the current controller bandwidth, meaning that the source impedance is higher at the cable resonant frequencies therefore Z_s and Z_L do not cross at frequencies where the combined phase is close to -180°. Higher frequency resonances for longer cables tend to be more damped than lower frequency resonances meaning that the load phase at higher frequencies is not close to 90°. This means the minor loop will not cross -180°.

5. Time Domain Simulations

Time domain simulations are performed to verify the harmonic stability analysis. The offshore wind farm is connected to shore via an LFAC cable. Onshore the BtB converter consists of the voltage controlled converter on the LFAC side and a DC voltage controlled power port on the 50 Hz side. The inner current and outer voltage controllers are as outlined in Figures 2a and 2b and average models of the converters are used. Figure 19 shows the three phase circuit setup used to perform the simulations.
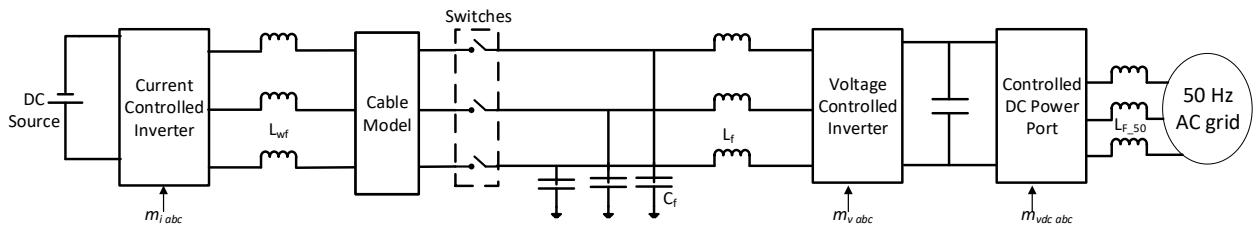
16

Figure 19: Three phase circuit layout for harmonic stability time domain simulations.

Initially the LFAC cable is not connected to the BtB converter. The voltage controller brings the AC voltage at the terminals of the VSC to 100 kV. At t = 0.3 s the switches are closed, LFAC cable is switched into service and the offshore wind farm is connected to the onshore grid. This is done to allow any start-up transients to dissipate and show that the system has no harmonic instability without the cable connected.
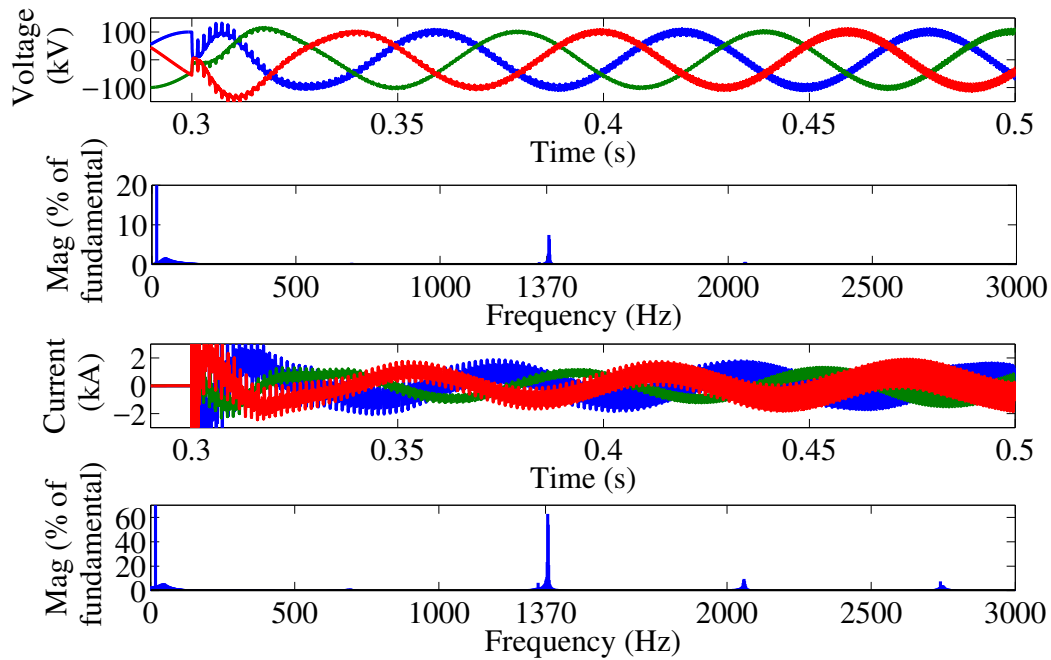

Figure 20: Voltage, Current and FFT of Voltage showing harmonic instability for $11\mu F$ capacitor and 100 km LFAC cable with a current control bandwidth of 2000 rads^{-1}.

Figure 20 displays the results of the unstable case with the 2000 rads^{-1} current control bandwidth in Figure 17. The LFAC voltage and current at the voltage controlled inverter terminals is shown, with the FFT of each below. The FFT is taken for the first 10 cycles (0.6 s) after the cable is switched in. In Figures 14 and 17 it was shown that the minor loop plot crosses 0 dB at 1370 Hz with a phase of -182°indicating that the voltage controlled inverter will be unstable. It can be seen from Figure 20 that the system is unstable and has a large

17

high frequency harmonic instability at 1370 Hz. Less significant harmonic components can be seen in the current at the other points where the source and load impedance cross each other.

Figure 21 shows the response of a stable LFAC system for the case with lower current control bandwidth in Figure 17 without any harmonic instability present. The cable is connected and after a brief transient normal operation begins and the offshore wind farm is connected to the grid. It can be seen from the FFT of the current that there are harmonic components in the initial transient at all the frequencies which the source and load impedance cross in Figure 16. These simulations verify the accuracy of the impedance based approach for predicting potential harmonic instability in an LFAC transmission system
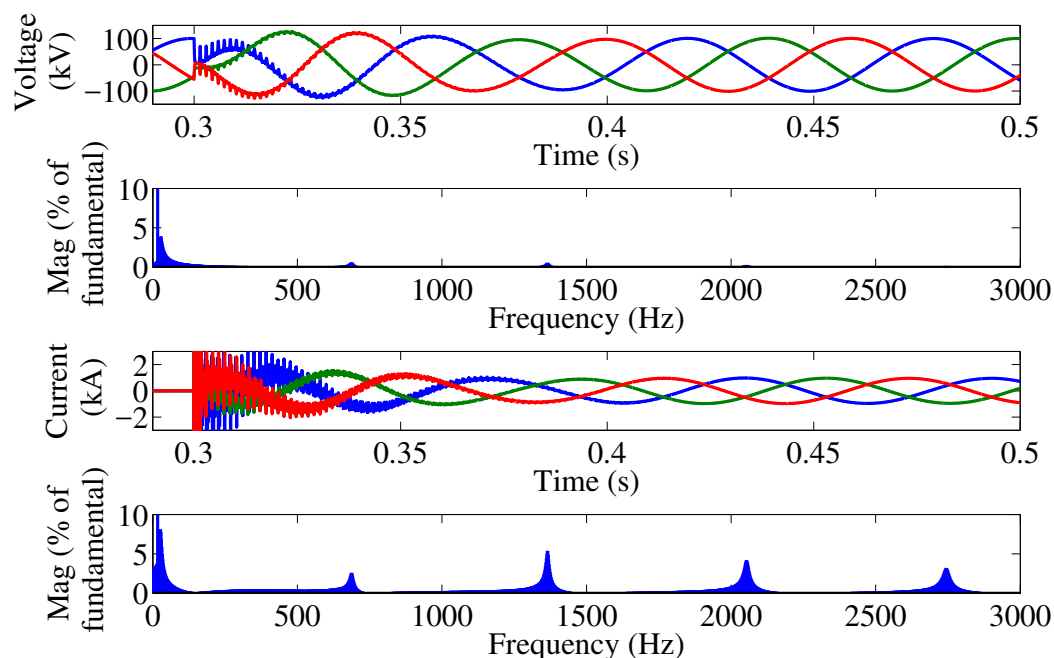

Figure 21: Voltage, Current and FFT of Voltage showing for $11\mu F$ capacitor and 100 km LFAC cable with a current control bandwidth of 1000 rads[1].

6. Hardware Experiment Result

In order to further verify the impedance based harmonic stability analysis, a 100 V, 2 kVA scaled prototype of the LFAC system has been implemented with the hardware in the loop real-time simulation platform from OPAL-RT. The LFAC transmission system hardware setup schematic is similar to the one described in Figure 19. The hardware setup shown in Figure 22, includes the OPAL-RT system implementing the control, the converters, their filters, and the LFAC cable. The offshore wind farm is modelled as a 300 V DC source connected to the current controlled inverter. The BtB converter is comprised of two 2 kVA

Parameter	Value
Voltage Controller Bandwidth (ω_c) in high/low case	334.2 rads^{-1} / 111.5 rads^{-1}
Voltage Controller (K_p,K_i) in high/low case	0.09, 9.97 / 0.27, 29.9
Current Controller Bandwidth ($\frac{1}{t_i}$)	1000 rads^{-1}
Current Controller (K_p,K_i)	33.02, 169.9
PWM frequency	1352.7 Hz
Filter Inductance (L$_f$, r$_f$)	33 mH, 126 mΩ
Filter Capacitance (C$_f$)	4.03 μF
Cable Inductance	80 μH/km
Pi section (L+r$_L$,C)	71.9 μH + 63.6 mΩ, 71.9μF
BtB DC voltage	500 V
V$_{sd}$ref, V$_{sq}$ref	100 V, 0 V
P$_{ref}$, Q$_{ref}$	1000 W, 1000 VA

Table 3: LFAC transmission system parameters for the hardware experiment.

VSCs, with a 680 μF capacitor on the DC link. The cable is implemented as 5 pi sections. Table 3 gives the parameters of the hardware system. In this section, we use the hardware to verify the impact of voltage controller bandwidth which is analysed in section 4.2 on the harmonic stability. The compared voltage controller bandwidths are 334.2 rads^{-1} and 111.5 rads^{-1} with corresponding PI gains given in Table 3.
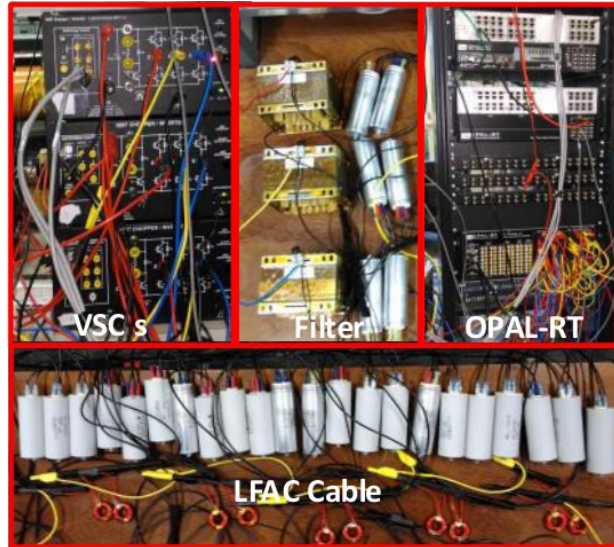

Figure 22: Picture of hardware setup.

Figures 23 and 24 show the measured time domain voltage and current waveforms and a Fourrier analysis of the current, for both a stable and unstable case , with the real/reactive power flow at 1000 W/1000 VA. The stable case corresponds to the higher voltage controller

19

bandwidth and the unstable case has the lower bandwidth. It can be seen that for the stable case the only significant harmonics present are those associated with the switching frequency at 1.3 kHz. For the unstable case these is a considerable oscillation present in the current at approximately 550 Hz.
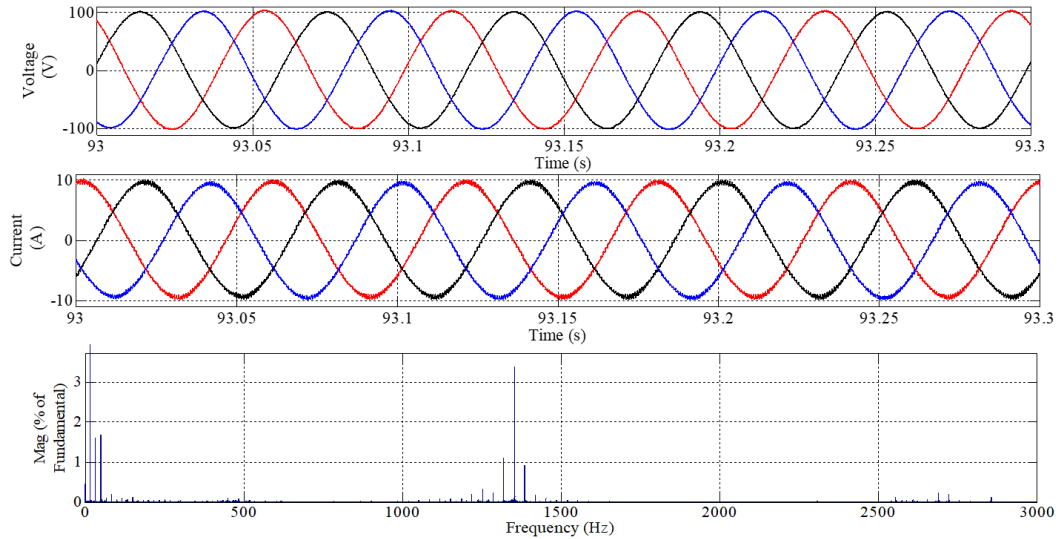
Figure 23: Measured Voltage, Current and FFT showing stable for high voltage controller bandwidth ω_c=334.2 rads^{-1}.
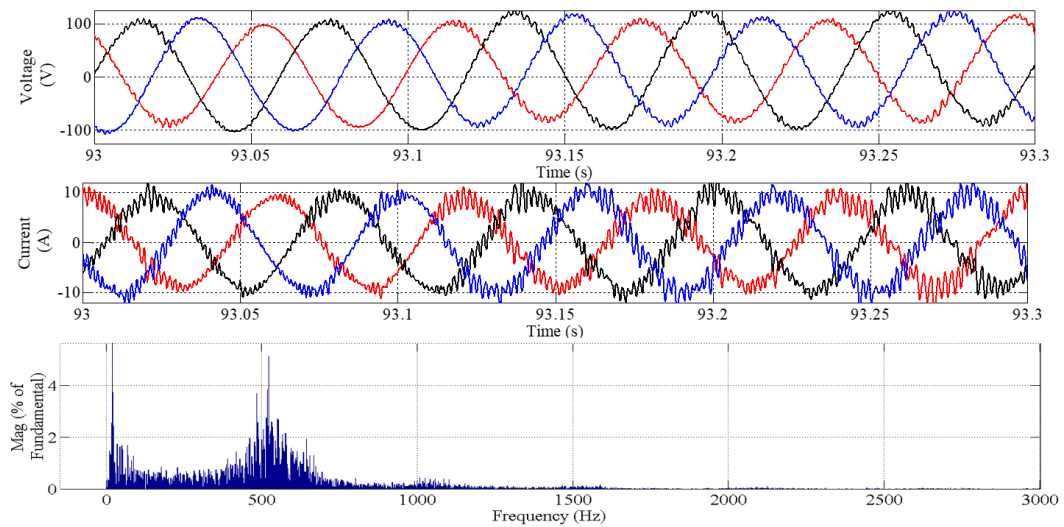

Figure 24: Voltage, Current and FFT showing harmonic unstable for low voltage controller bandwidth ω_c=111.5 rads^{-1}.

The corresponding minor loop responses of the tested hardware cases are shown in Figure 25. These are generated from a Matlab/Simulink model using the hardware paramters in

Table 3. These plots indicate that the minor loop for low voltage controller bandwidth crosses 0 dB at 538 Hz with a phase of -181 indicating an instability which matches closely with the current oscillation observed in the measured response. On the other hand the minor loop associated with the high voltage controller bandwidth indicates that it is stable which is again reflected in the hardware measurements.
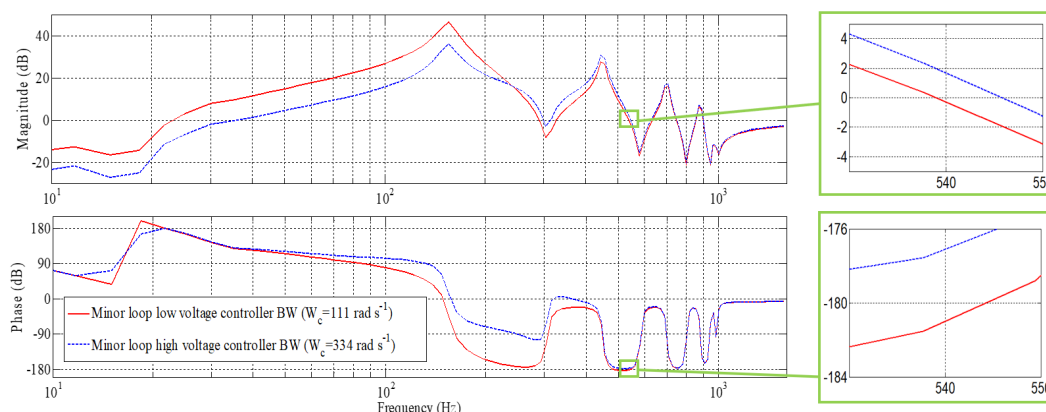

Figure 25: Minor loop responses with varied voltage controller bandwidth analysed by Simulink with the hardware experiment parameters, which indicates that it is unstable for low voltage controller bandwidth and stable for high voltage controller bandwidth.

7. Conclusion

This paper has examined in detail the stability of an LFAC transmission system via impedance analysis and 3 phase simulations. The impedance scan methodology is used to determine the harmonic stability of the LFAC transmission system. The impact of different control parameters and filter sizes on stability is examined. It is found that decreasing the magnitude of the voltage controlled converter source impedance by increasing either the current controller bandwidth or the filter capacitor size can have an adverse effect on harmonic stability. It is clear that control parameters, particularly current control bandwidth can have an effect on harmonic stability by changing the source impedance Z_S. The voltage control bandwidth has little impact on harmonic stability as it's influence is at lower frequency. In the LFAC system Z_L will generally not change at high frequencies as it is only influenced by cable length. To mitigate harmonic stability issues Z_S can be adapted, either by varying the filter components, or the controller bandwidths. It is also found that shorter LFAC cables are more susceptible to harmonic instability than longer cables since with the longer cables the resonant points are at lower frequency and therefore usually within or close to the current controller bandwidth. This causes the source and load impedance scans not to intersect at any frequency where the combined phase may be close to -180°. The obvious caveat is that longer cables require significantly more reactive power compensation. A proportional resonant filter could help mitigate harmonic stability issues however perfect knowledge of the resonant frequencies is required and the movement of resonant frequencies due to changes in grid conditions must be taken into account.

It is clear there is no substitute for having complete knowledge of the system and performing detailed 3 phase simulation studies and eigenvalue analysis for a range of disturbance scenarios to determine stability issues. However as mentioned this may not always be the case. Impedance based stability analysis can be used as a practical approach to determine the stability of an inverter based system, where complete information of system parameters is not always available. A major problem for system planners is the black box nature of control systems around both the wind turbine and the large substation converters. Models will be provided by the manufactures however it is not always possible that accurate voltage/current controller parameters will be known. It is important for system planners to determine the harmonic stability of the system in the design stage, so that controls can be adjusted to mitigate these issues.

8. References

[1] W. Fischer, R. Braun, and I. Erlich, "Low frequency high voltage offshore grid for transmission of renewable power," in *3rd IEEE PES Innovative Smart Grid Technologies Europe*, Oct. 2012.

[2] T. Funaki and K. Matsuura, "Feasibility of the low frequency AC transmission," in *IEEE Power Engineering Society Winter Meeting*, vol. 04, 2000, pp. 2693–2698.

[3] H. Chen, M. H. Johnson, and D. C. Aliprantis, "Low-Frequency AC Transmission for Offshore Wind Power," *IEEE Trans. Power Del.*, vol. 28, no. 4, pp. 2236–2244, 2013.

[4] E. Olsen, U. Axelsson, and A. Canelhas, "Low Frequency AC Transmission on large scale Offshore Wind Power Plants, Achieivng the best from two worlds?" in *13th Wind Integration Workshop*, Berlin, Germany, 2014.

[5] J. Ruddy, R. Meere, and T. O'Donnell, "Low Frequency AC transmission for offshore wind power: A review," *Renewable and Sustainable Energy Reviews*, vol. 56, pp. 75–86, 2016.

[6] X. Wang, F. Blaabjerg, and W. Wu, "Modeling and Analysis of Harmonic Stability in an AC Power-Electronics-Based Power System," *IEEE Transactions on Power Electronics*, vol. 29, no. 12, pp. 6421–6432, 2014.

[7] CIGRE working group B4.62, "Technical Brochure 671 Connection of Wind Farms to Weak AC Networks," Tech. Rep. December, 2016.

[8] C. Buchhagen, C. Rauscher, A. Menze, and J. Jung, "BorWin1 - First Experiences with harmonic interactions in converter dominated grids," in *International ETG Congress 2015; Die Energiewende - Blueprints for the new energy age*, 2015, pp. 1–7.

[9] W. Ren and E. Larsen, "A Refined Frequency Scan Approach to Sub-Synchronous Control Interaction (SSCI) Study of Wind Farms," *IEEE Transactions on Power Systems*, vol. 31, no. 5, pp. 3904–3912, 2016.

[10] G. Gaba, S. Lefebvre, and D. Mukhedkar, "Comparative analysis and study of the dynamic stability of ac/dc systems," *IEEE Transactions on Power Systems*, vol. 3, no. 3, pp. 978–985, Aug 1988.

[11] J. Sun, "Impedance-Based Stability Criterion for Grid-Connected Inverters," *IEEE Transactions on Power Electronics*, vol. 26, no. 11, pp. 3075–3078, 2011.

[12] M. Cespedes and J. Sun, "Adaptive control of grid-connected inverters based on online grid impedance measurements," *IEEE Transactions on Sustainable Energy*, vol. 5, no. 2, pp. 516–523, 2014.

[13] W. Cao, Y. Ma, and F. Wang, "Sequence-Impedance-Based Harmonic Stability Analysis and Controller Parameter Design of Three-Phase Inverter-Based Multibus AC Power Systems," *IEEE Transactions on Power Electronics*, vol. 32, no. 10, pp. 7674–7693, 2017.

[14] A. Rygg, M. Molinas, C. Zhang, and X. Cai, "A Modified Sequence-Domain Impedance Definition and Its Equivalence to the dq-Domain Impedance Definition for the Stability Analysis of AC Power Electronic Systems," *IEEE Journal of Emerging and Selected Topics in Power Electronics*, vol. 4, no. 4, pp. 1383–1396, 2016.

[15] M. Amin and M. Molinas, "Non-parametric impedance based stability and controller bandwidth extraction from impedance measurements of hvdc-connected wind farms," *arXiv preprint arXiv:1704.04800*, 2017.

[16] B. Wen, D. Dong, D. Boroyevich, R. Burgos, P. Mattavelli, and Z. Shen, "Impedance-based analysis of grid-synchronization stability for three-phase paralleled converters," *IEEE Transactions on Power Electronics*, vol. 31, no. 1, pp. 26–38, Jan 2016.

[17] H. Liu and J. Sun, "Voltage Stability and Control of Offshore Wind Farms With AC Collection and HVDC Transmission," *IEEE Journal of Emerging and Selected Topics in Power Electronics*, vol. 2, no. 4, pp. 1181–1189, 2014.

[18] M. Amin, M. Molinas, and J. Lyu, "Oscillatory phenomena between wind farms and HVDC systems: The impact of control," in *2015 IEEE 16th Workshop on Control and Modeling for Power Electronics (COMPEL)*, 2015, pp. 1–8.

[19] T. Roinila, M. Vilkko, and J. Sun, "Online grid impedance measurement using discrete-interval binary sequence injection," *IEEE Journal of Emerging and Selected Topics in Power Electronics*, vol. 2, no. 4, pp. 985–993, Dec 2014.

[20] M. Amin, A. Rygg, and M. Molinas, "Impedance-based and eigenvalue based stability assessment compared in VSC-HVDC system," in *2016 IEEE Energy Conversion Congress and Exposition (ECCE)*, 2016, pp. 1–8.

[21] Z. Shen, "Online measurement of three-phase ac power system impedance in synchronous coordinates," Ph.D. dissertation, Virginia Polytechnic Institute and State University, 2013.

[22] R. D. Middlebrook, "Input filter considerations in design and application of switching regulators," in *in Conf. Rec. IEEE IAS Annual Meeting*, 1979, pp. 366–382.

[23] C. M. Wildrick, F. C. Lee, B. H. Cho, and B. Choi, "A method of defining the load impedance specification for a stable distributed power system," *IEEE Transactions on Power Electronics*, vol. 10, no. 3, pp. 280–285, May 1995.

[24] D. Yang, X. Wang, and F. Blaabjerg, "Sideband harmonic instability of paralleled inverters with asynchronous carriers," *IEEE Transactions on Power Electronics*, vol. 33, no. 6, pp. 4571–4577, June 2018.

[25] M. A. Salman and C. S. Edrington, "Real-time small signal stability analysis of the power electronics based components in contemporary distribution systems," *Electric Power Systems Research*, vol. 117, pp. 47–58, dec 2014.

[26] L. Xu, L. Fan, and Z. Miao, "Dc impedance-model-based resonance analysis of a vsc x2013;hvdc system," *IEEE Transactions on Power Delivery*, vol. 30, no. 3, pp. 1221–1230, June 2015.

[27] G. Pinares and M. Bongiorno, "Modeling and analysis of vsc-based hvdc systems for dc network stability studies," *IEEE Transactions on Power Delivery*, vol. 31, no. 2, pp. 848–856, April 2016.

[28] W. Wu, Y. Chen, L. Zhou, X. Zhou, L. Yang, Y. Dong, Z. Xie, and A. Luo, "A virtual

phase-lead impedance stability control strategy for the maritime vsc-hvdc system," *IEEE Transactions on Industrial Informatics*, pp. 1–1, 2018.

[29] M. Amin, M. Molinas, J. Lyu, and X. Cai, "Impact of power flow direction on the stability of vsc-hvdc seen from the impedance nyquist plot," *IEEE Transactions on Power Electronics*, vol. 32, no. 10, pp. 8204–8217, Oct 2017.

[30] X. Wang and F. Blaabjerg, "Harmonic stability in power electronic based power systems: Concept, modeling, and analysis," *IEEE Transactions on Smart Grid*, pp. 1–1, 2018.

[31] A. Yazdani and R. Iravani, *Voltage-Sourced Converters in Power Systems Modeling, Control and Applications.* John Wiley and sons Inc, 2010.

[32] J. Jokipii, T. Messo, and T. Suntio, "Simple method for measuring output impedance of a three-phase inverter in dq-domain," in *2014 International Power Electronics Conference (IPEC-Hiroshima 2014 - ECCE ASIA)*, 2014, pp. 1466–1470.